Cellular/Molecular

The Contribution of Blood Lactate to Brain Energy Metabolism in Humans Measured by Dynamic ^{13}C Nuclear Magnetic Resonance Spectroscopy

Fawzi Boumezbeur,[1,6] Kitt F. Petersen,[2] Gary W. Cline,[2] Graeme F. Mason,[1,3] Kevin L. Behar,[1,3] Gerald I. Shulman,[2,5] and Douglas L. Rothman[1,4]

Departments of [1]Diagnostic Radiology, [2]Internal Medicine, [3]Psychiatry, and [4]Biomedical Engineering, Yale School of Medicine, and [5]Department of Cellular and Molecular Physiology, Howard Hughes Medical Institute, Yale School of Medicine, New Haven, Connecticut 06520, and [6]NeuroSpin, Institute d'Imagerie Biomédicale, Commissariat à l'Energie Atomique, 91191 Gif-sur-Yvette Cedex, France

To determine whether plasma lactate can be a significant fuel for human brain energy metabolism, infusions of [3-^{13}C]lactate and ^{1}H-^{13}C polarization transfer spectroscopy were used to detect the entry and utilization of lactate. During the 2 h infusion study, ^{13}C incorporation in the amino acid pools of glutamate and glutamine were measured with a 5 min time resolution. With a plasma concentration ($[Lac]_P$) being in the 0.8–2.8 mmol/L range, the tissue lactate concentration ($[Lac]_B$) was assessed as well as the fractional contribution of lactate to brain energy metabolism (CMRlac). From the measured relationship between unidirectional lactate influx (V_{in}) and plasma and brain lactate concentrations, lactate transport constants were calculated using a reversible Michaelis–Menten model. The results show that (1) in the physiological range, plasma lactate unidirectional transport (V_{in}) and concentration in tissue increase close to linearly with the lactate concentration in plasma; (2) the maximum potential contribution of plasma lactate to brain metabolism is 10% under basal plasma lactate conditions of ~1.0 mmol/L and as much as 60% at supraphysiological plasma lactate concentrations when the transporters are saturated; (3) the half-saturation constant K_T is 5.1 ± 2.7 mmol/L and V_{MAX} is 0.40 ± 0.13 μmol · g^{-1} · min^{-1} (68% confidence interval); and (4) the majority of plasma lactate is metabolized in neurons similar to glucose.

Introduction

In the traditional view of brain energy metabolism, glucose is the predominant energy substrate (Siesjö, 1978) with lactate returned to the circulation as a metabolic by-product of glycolytic (nonoxidative) excess. Under normal resting conditions, lactate is present in the blood at a concentration of ~0.5–1.0 mmol/L and the brain is a small net exporter of lactate (Siesjö, 1978; Sokoloff, 1989; Harada et al., 1992). However, lactate can cross the blood–brain barrier through monocarboxylate transporters (MCTs) (Oldendorf, 1973; Simpson et al., 2007), and recent studies have provided evidence that lactate can become a significant fuel source when elevated in the blood (Smith et al., 2003; van Hall et al., 2009). Plasma lactate may also be an important fuel source for the brain during hypoglycemia. Maran et al. (1994) reported that infusion of lactate allows maintenance of normal human brain evoked potentials during hypoglycemia. Recently, we reported that acetate transport from blood to brain, which involves monocarboxylate transporters, was greater in subjects with well controlled type 1 diabetes. We hypothesized that plasma lactate could potentially be an important net fuel source during insulin-induced hypoglycemia (Mason et al., 2006). Furthermore, there is evidence from *in vitro* and *in vivo* experiments that lactate may be required energetically to support synaptic function (for review, see Pellerin et al., 2005), potentially via shuttling of glycolytically derived carbons from astroglia to neurons (Magistretti et al., 1999; Pellerin et al., 2005) for oxidation.

Combined with ^{13}C-labeled substrates and appropriate metabolic modeling, nuclear magnetic resonance spectroscopy (MRS) allows for noninvasive measurement of metabolic fluxes in human brain based on the dynamic detection of ^{13}C incorporation into the large cerebral pools of glutamate and glutamine (Rothman et al., 1992; Gruetter et al., 1994, 2001; Lebon et al., 2002; Lin et al., 2003). Human cerebral metabolism of ^{13}C-labeled glucose, acetate (Blüml et al., 2002; Lebon et al., 2002), and β-hydroxybutyrate (Pan et al., 2000, 2001, 2002) have been investigated with ^{13}C or ^{1}H-{^{13}C} MRS (for review, see Shen and Rothman, 2002; Hyder et al., 2006). In this report, we describe the first use of 3-^{13}C-labeled lactate with *in vivo* ^{13}C MRS to directly assess transport kinetics and metabolism of plasma lactate in the human cerebral occipital cortex, as well as estimate the relative contributions of plasma lactate to neuronal and glial metabolism.

Received April 21, 2010; revised June 9, 2010; accepted Aug. 2, 2010.

This work was supported by National Institutes of Health (NIH) Grants R01-NS037527 (D.L.R.), K02-AA13430 (G.F.M.), R01-AG23686 (K.F.P.), and P01-DK68229 (G.I.S., K.F.P., D.L.R.), Howard Hughes Medical Institute (G.I.S.), The Keck Foundation, and NIH/National Center for Research Resources/General Clinical Research Center/M01-RR00125. We thank Mikhail Smolgovsky, Yanna Kosover, Donna D'Eugenio, Gina D'Agostino, and the Yale/New Haven Hospital General Clinical Research Center for their technical assistance; Terry Nixon, Peter Brown, and Scott McIntyre for maintenance and upgrades to the MRS system; and the volunteers for their participation in these studies.

Correspondence should be addressed to Dr. Fawzi Boumezbeur, NeuroSpin, I2BM, Commissariat à l'Energie Atomique, Centre de Saclay, Bâtiment 145, 91191 Gif-sur-Yvette Cedex, France. E-mail: fawzi.boumezbeur@cea.fr.

DOI:10.1523/JNEUROSCI.2040-10.2010

Copyright © 2010 the authors 0270-6474/10/3013983-09$15.00/0

Materials and Methods

Subjects

Seven young healthy volunteers [four females, three males; age, 24 ± 1; mean ± SD, body mass index (BMI), 24 ± 1 kg/m^2] were recruited for this study. Written consent was obtained from each subject after the purpose and potential risks were explained. The protocol was approved by the Yale University Human Investigation Committee. They were all healthy, lean nonsmokers and taking no medications. All subjects underwent a complete medical history and physical examination along with blood tests to verify normal hemoglobin, hematocrit, electrolytes, aspartate aminotransferase, alanine aminotransferase, blood urea nitrogen, creatinine, cholesterol, and triglycerides. Nine MRS studies were performed according to two different infusion protocols (A and B) designed to rapidly raise and maintain plasma lactate ^{13}C fractional enrichment (fe[LacC3]$_P$) to either (A) 33% while maintaining plasma lactate concentration ([Lac]$_P$) at close to physiological levels (~1.5 mmol/L) or (B) 50% while maintaining plasma lactate at twice the physiological levels (~2.5 mmol/L).

After an overnight fast, an intravenous catheter was placed in an antecubital vein in each arm for the infusion and for blood sampling. After placement of catheters, the subject was positioned within the magnet, and acquisition optimization was performed. After acquisition of the baseline spectrum, [3-^{13}C]lactate was infused (350 mmol/L sodium salt 99% ^{13}C enriched; Cambridge Isotopes) at either (A) a priming dose of 150 μmol/kg given over 5 min followed by a continuous infusion of 10 μmol · kg^{-1} · min^{-1} for ~120 min, or (B) a priming dose of 300 μmol/kg given over 5 min followed by a continuous infusion of 20 μmol · kg^{-1} · min^{-1} for ~120 min. Each volunteer underwent either protocol A or B, and two subjects underwent both, leading to a total of 12 experiments, of which 9 were used for kinetic analysis.

MRS acquisition

MRS data were acquired on a 4.0 T whole-body magnet interfaced to a Bruker AVANCE spectrometer (Bruker Instruments). Subjects were placed supine in the magnet, with the head immobilized with foam, lying on top of a radiofrequency probe consisting of one ^{13}C circular coil (8.5 cm diameter) and two ^{1}H quadrature coils for acquisition and decoupling. After tuning, acquisition of scout images, shimming with the FASTERMAP procedure (Shen et al., 1997) and calibration of decoupling power, ^{13}C spectra were acquired before and during the [3-^{13}C]lactate infusion using a localized adiabatic ^{13}C-{^{1}H} refocused INEPT sequence optimized for glutamate and glutamine in the C4 position using 3D-ISIS combined with outer volume saturation for localization on the ^{1}H magnetization (Shen et al., 1999) (128 transients; repetition time: 2.5 s; 5.3 min time resolution). The spectroscopic volume was located in the occipital-parietal lobe, with its size adapted to each volunteer and was on average 106 ± 1.6 ml (mean ± SD; $n = 9$).

Data processing

MRI segmentation. The tissue composition of each voxel was determined from T$_1$-based image segmentation maps according to a previously described protocol (Hetherington et al., 1996; Mason and Rothman, 2002). Briefly, sets of B$_1$ maps and inversion-recovery images were acquired and processed to yield quantitative T$_1$ maps, which were converted to segmented images of gray matter, white matter, and CSF. The gray matter volume was 47 ± 1.8% of tissue content in the voxel (mean ± SD; $n = 9$).

Spectral analysis. All the spectra were analyzed using LCModel 6.1 (Provencher, 1993) (Stephen Provencher Inc.) modified to process ^{13}C spectral data as explained by Henry et al. (2003). The LCModel basis set was generated by simulating spectra for every observable isotopomer with NMRSim 2.8 (Bruker Analytik) using published values of ^{13}C chemical shifts and homonuclear ^{13}C-^{13}C coupling constants (J_{CC}) from Henry et al. (2003). Resonances quantified included the C3 position of aspartate (AspC3), the C2, C3, and C4 positions of glutamate (GluC2, GluC3, GluC4) and glutamine (GlnC2, GlnC3, GlnC4), the C3 position of *N*-acetyl aspartate (NAAC3), and the C3 position of lactate (LacC3). The spectra were added three by three in running averages of 16 min to increase the signal-to-noise ratio (SNR) before processing. A 3 Hz Gaussian apodization and zero-filling to 8k data points were applied to all the spectra before the LCModel analysis. Relative concentrations obtained from LCModel were converted to absolute concentrations by referring to the natural abundance (1.1%) signal of NAAC3 assuming a NAA pool size of 11 μmol/g in the voxel, based on ^{1}H MRS measurements from a similar region (Michaelis et al., 1993; Mangia et al., 2006). Calibration of the basis set to account for differences in polarization transfer efficiency and off-resonance effects were realized using a series of phantom experiments (data not shown). For the very first time points, because of low SNR, systematic overestimations were apparent; to avoid them, for the first 30 min, peak heights were determined manually and scaled on the last spectra. In addition, to improve reliability, only the singlet signals were considered for glutamate (GluC4, GluC3, and GluC2) and glutamine (GlnC4, GlnC3, and GlnC2). Based on probabilities of obtaining double and triply labeled isotopomers, correction factors were calculated and applied to account for the contribution of these isotopomers (GluC43, GluC32, GluC234, GlnC43, GlnC32, and GlnC234).

Measurement of brain lactate concentration. The brain lactate concentration was determined from the measured concentration of ^{13}C3 lactate ([LacC3]$_B$) by assuming that the lactate fractional C3 fractional enrichment (fe[LacC3]$_B$) was the same as that of glutamate C4 at steady state (fe[GluC4]), as a consequence of the lactate/pyruvate pool being the immediate precursor for acetyl-CoA, which is the precursor for the glutamate C4 and C5 carbons (Mason et al., 1995), as follows:

$$[\mathrm{Lac}]_B = \frac{[\mathrm{LacC3}]_B}{\mathrm{fe}[\mathrm{LacC3}]_B} = \frac{[\mathrm{LacC3}]_B}{\mathrm{fe}[\mathrm{GluC4}]}. \quad (1)$$

Metabolic modeling analysis

^{13}C Time courses, modeling, and metabolic fluxes determination. Previous labeling experiments have established that cerebral metabolism can be characterized by two distinct metabolic compartments associated to neurons and glial cells (Lebon et al., 2002, and references therein). ^{13}C Labeling time courses for glutamate and glutamine in the C4, C3, and C2 positions and the C3 position of lactate were fitted according to this two-compartment metabolic model (Gruetter et al., 2001; Lebon et al., 2002; Henry et al., 2006) using Matlab (The MathWorks) and CWave (Mason et al., 2003) with time courses for plasma lactate and glucose concentrations and ^{13}C fractional enrichments as input functions. Values for the rates of neuronal and glial tricarboxylic acid (TCA) cycles (noted V_{TCAn} and V_{TCAg}, respectively) and the unidirectional rate of lactate uptake (V_{in}) were estimated using a simulated annealing algorithm. The neuronal/astroglial glutamate/glutamine cycle (V_{cycle}) was defined as 0.33 of V_{TCAn} according to previous infusion studies in humans (Lebon et al., 2002). The mitochondrial/cytosolic glutamate/α-ketoglutarate exchange rate in neurons and astrocytes (V_{Xn} and V_{Xg}) were fitted to improve the accuracy of the TCA cycle rates determination (Mason et al., 1992; Gruetter et al., 2001). Pyruvate carboxylase activity (V_{PC}) was considered equal to 0.06 of V_{cycle} based on the value reported previously by Mason et al. (2007) after infusion of [2-^{13}C]glucose in humans. The concentrations of glutamate and glutamine used for the modeling were assumed to be 9.1 and 4.1 μmol/g, respectively, as reported previously by MRS in a similar volume (Gruetter et al., 1994).

To estimate the early time course of the brain lactate fractional enrichment, a reversible Michaelis–Menten model of lactate transport was used (see below). A K_T of 4.4 mmol/L was assumed based on previous characterization of MCT transporters (Bröer et al., 1998; Manning Fox et al., 2000). Iteration was done with the values of V_{MAX} and K_T to obtain the least-squares fit of the measured time courses. To assess whether the transport parameters would have a significant impact on the calculated metabolic rates, we performed fits of the data using K_T values covering the full range compatible with the results (see Results). Because of the small size of the lactate pool relative to the large metabolic flux passing through it (glycolysis and lactate transport), the value of K_T had minimal impact on the derived rates since in all cases the brain lactate pool rapidly achieved isotopic steady state relative to the labeled precursor.

To account for the probable contribution of the circulating ^{13}C-labeled lactate to the overall [3-^{13}C]lactate signal, a vascular fraction of 3–5% of the total volume was calculated for each experiment according to the voxel composition leading to the subsequent correction (Leenders et al., 1990). In addition, to take into account any scrambling of label lactate into plasma glucose by the liver, the plasma glucose C1 and C6 labeling time courses were used as an input function along with the fractional enrichment of plasma C3 lactate.

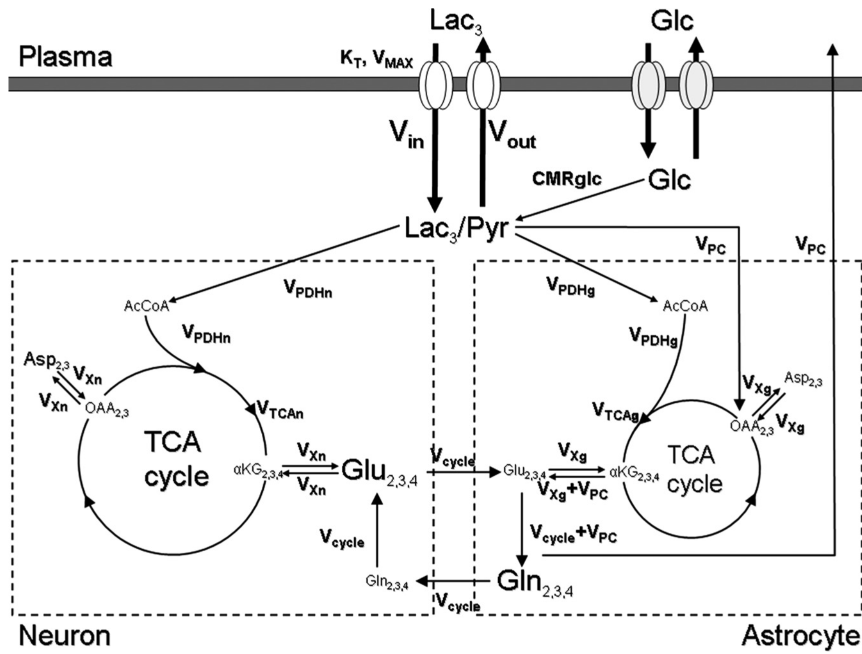

Figure 1. Two-compartment model describing the incorporation of label from [3-^{13}C]lactate into the brain glutamate and glutamine pools. Left, Neuronal compartment; right, astroglial compartment. Lac, Lactate; Glc, glucose; Pyr, pyruvate; AcCoA, acetyl coenzyme A; OAA, oxaloacetate; αKG, α-ketoglutarate; Glu, glutamate; Gln, glutamine; Asp, aspartate; V_{in}, influx of lactate; V_{out}, efflux of lactate; CMRglc, glucose consumption; V_{PDHn}, neuronal flux through the pyruvate dehydrogenase; V_{PDHg}, astroglial flux through the pyruvate dehydrogenase; V_{TCAn}, neuronal TCA cycle rate; V_{TCAg}, astroglial TCA cycle rate; V_{PC}, flux through the pyruvate carboxylase; V_{cycle}, glutamate/glutamine cycle flux; V_{Xn}, mitochondrial/cytosolic glutamate/α-ketoglutarate exchange rate in neurons; V_{Xg}, mitochondrial/cytosolic glutamate/α-ketoglutarate exchange rate in astrocytes. In our experiment, ^{13}C-labeled lactate cross the blood–brain barrier back and forth through the monocarboxylate transporters (K_T, V_{MAX}) and arrives at the C3 of the lactate/pyruvate pool (regrouped as a unique pool because of the very fast exchange between them through the lactate dehydrogenase), where the label enters the TCA cycle via pyruvate carboxylase or pyruvate dehydrogenase reaction. It is ultimately detected at the first turn of the TCA cycle in the C4 position of glutamate and glutamine then, after label scrambling by the TCA activity, on the C2 and C3 positions of glutamate and glutamine.

Modeling of lactate transport kinetics and calculation of K_T *and* V_{MAX}/K_T. To model lactate transport, we used a reversible Michaelis–Menten model (Fig. 1). The physical distribution space of lactate was assumed to be similar to glucose at $V_d = 0.77$ mg/dl (Gjedde and Diemer, 1983; Gruetter et al., 1996). The reversible Michaelis–Menten kinetics have been described in detail previously (Mahler and Cordes, 1971; Cunningham et al., 1986) and used successfully to study glucose transport kinetics in human brain (Gruetter et al., 1998; Choi et al., 2001; de Graaf et al., 2001). Detailed kinetic modeling and meta-analysis of literature results by Simpson et al. (2007) have supported it as accurately describing brain glucose and monocarboxylic acid transport. At steady state, the reversible Michaelis–Menten model results in the following expressions for the influx (V_{in}), efflux (V_{out}), the net consumption of lactate (CMRlac), and the brain lactate level ($[\mathrm{Lac}]_B$):

$$V_{in} = V_{MAX}\frac{[\mathrm{Lac}]_P}{K_T + [\mathrm{Lac}]_P + [\mathrm{Lac}]_B}, \tag{2}$$

$$V_{out} = V_{MAX}\frac{[\mathrm{Lac}]_B}{K_T + [\mathrm{Lac}]_P + [\mathrm{Lac}]_B}, \tag{3}$$

$$\mathrm{CMRlac} = V_{in} - V_{out} = V_{TCA} - 2.\mathrm{CMRglc}, \tag{4}$$

$$[\mathrm{Lac}]_B = \frac{\left(\frac{V_{MAX}}{\mathrm{CMRlac}} - 1\right)[\mathrm{Lac}]_P - K_T}{\frac{V_{MAX}}{\mathrm{CMRlac}} + 1}. \tag{5}$$

The last expression predicts that $[\mathrm{Lac}]_B$ is a linear function of plasma lactate level ($[\mathrm{Lac}]_P$) when CMRlac is constant. Equations 2 and 3 can be combined, resulting in the following:

$$\frac{V_{in}}{V_{out}} = \frac{[\mathrm{Lac}]_P}{[\mathrm{Lac}]_B} \tag{6}$$

$$\mathrm{CMRlac} = V_{in}\left(1 - \frac{[\mathrm{Lac}]_B}{[\mathrm{Lac}]_P}\right). \tag{7}$$

Thus, Equation 2 can be rearranged, yielding the following:

$$V_{in} = \frac{V_{MAX}}{K_T}\frac{[\mathrm{Lac}]_P}{1 + ([\mathrm{Lac}]_P + [\mathrm{Lac}]_B)/K_T}. \tag{8}$$

From Equation 8, it is seen that V_{in} is highly sensitive to the V_{MAX}/K_T ratio and secondarily sensitive to the values V_{MAX} and K_T independently.

To estimate V_{MAX} and K_T and the corresponding uncertainty, we performed a Monte Carlo analysis based on the relationships of V_{in} and $[\mathrm{Lac}]_B$ versus $[\mathrm{Lac}]_P$ and the best fits of Equations 5 and 8 to the experimental data, using a least-squares minimization (see Fig. 6). For the Monte Carlo analysis, the noise was estimated as Gaussian distributions with SDs equal to the difference between the measured values and least-squares fitted values of V_{in} and $[\mathrm{Lac}]_B$. Random Gaussian noise with the same SD was added 100 times to the least-squares fitted values to create 100 noisy simulations of the data. The 100 simulated noisy sets were fitted to generate a list of 100 values of V_{MAX} and K_T, which were used to calculate SDs of their respective uncertainties (Mason et al., 1992).

Calculation of net lactate consumption. The net lactate consumption was calculated using the measured values of V_{in}, $[\mathrm{Lac}]_P$, $[\mathrm{Lac}]_B$, and Equation 7. Note that, as shown in the derivation of Equation 7 with the reversible Michaelis–Menten model, net consumption within our narrow range of plasma lactate levels can be derived from measurement of intracellular and plasma lactate and V_{in}.

Insensitivity of the calculation of V_{in} *to transport kinetics.* The unidirectional rate of lactate transport V_{in} was calculated from the ^{13}C labeling time courses (see above). Because assumed lactate transport parameters were used in the fitting to better fit the beginning of the time courses when brain lactate fractional enrichment was not at steady state, there is the possibility of circularity in which the assumed transport constants (at the initial iteration of the fits) biases the subsequent values calculated from the V_{in} plots. To test this possibility, the fits to the data were repeated considering the mean and probability distributions of K_T as determined from the Monte Carlo simulations, checking the fits over a range of $\pm$1 SD. In the end, over this range an effect of $<$1.4% was observed both on the calculated V_{in} and CMRlac values (see Fig. 7).

The reason for the insensitivity of the V_{in} measurement to lactate transport kinetics (K_T, V_{MAX}) can be shown by considering the relative fractional enrichment of plasma and brain lactate at steady state based on the relative fluxes in and out of the lactate pool as derived from the metabolic model in Figure 1 as follows:

$$\frac{\mathrm{fe}[\mathrm{GluC4}]}{\mathrm{fe}[\mathrm{LacC3}]_P} = \frac{\mathrm{fe}[\mathrm{LacC3}]_B}{\mathrm{fe}[\mathrm{LacC3}]_P} = \frac{V_{in}}{2.\mathrm{CMRglc} + V_{in}} = \frac{V_{in}}{V_{TCA} + V_{out}}. \tag{9}$$

By combining the relationships of Equations 9 and 6, one can derive the relationship of Equation 10 so that

$$V_{in} = V_{TCA}\left(\frac{\mathrm{fe}[\mathrm{LacC3}]_P}{\mathrm{fe}[\mathrm{GluC4}]} - \frac{[\mathrm{Lac}]_B}{V_d \cdot [\mathrm{Lac}]_P}\right)^{-1}. \tag{10}$$

As shown in Equation 10, there is sufficient information at steady state to calculate V_{in} from knowledge of the relative fractional enrichments and

concentrations of plasma and brain lactate at steady state and the rate of the brain TCA cycle without any influence of transport kinetics.

Blood sample processing. During the study, venous blood samples were withdrawn for glucose and lactate assays. Glucose assays were performed using a Beckman glucometer (Beckman); lactate assays were performed using an YSI 2300 analyzer. Fractional enrichment was determined by gas chromatography–mass spectroscopy. The distribution of ^{13}C label among the six glucose carbon atoms was then determined.

Comparison with studies that used [1-^{13}C]glucose and [2-^{13}C]acetate. Another group of eight healthy young subjects (three females, five males; age, 26 ± 7; mean ± SD, BMI, 23 ± 4 kg/m^2) underwent a set of [1-^{13}C]glucose and [2-^{13}C]acetate infusions. Spectra were obtained from the same occipito-parietal location and the respective data acquisition, infusion protocols, and data processing procedure were identical with those described here for the [3-^{13}C]lactate experiments. More detailed descriptions of the infusion protocols and analysis for this group have been given previously (Boumezbeur et al., 2010).

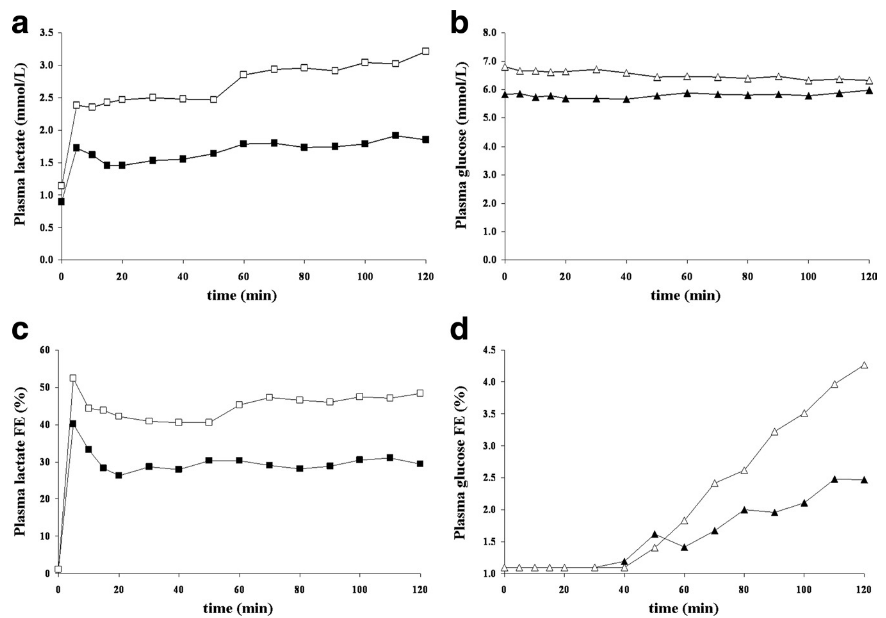

Figure 2. ***a–d***, Time courses of plasma lactate concentrations (***a***), glucose concentration (in millimoles per liter) (***b***), plasma lactate ^{13}C fractional enrichment (FE) (***c***), and glucose ^{13}C fractional enrichment (***d***) from the same volunteer for the two different infusion protocols A (black symbols) and B (white symbols). As aimed, plasma lactate level is either (protocol A) maintained close to a physiological level (~1.5 mmol/L) with a ^{13}C FE close to 33% or (protocol B) doubled (~2.5 mmol/L) with a ^{13}C FE close to 50%. Even if the plasma glucose level remains steady at euglycemic values, as the circulating [3-^{13}C]lactate is metabolized by the liver, ^{13}C atoms are progressively incorporated into the plasma glucose through gluconeogenesis.

Results

Plasma

Figure 2*a–d* shows typical plasma lactate ($[Lac]_P$) and glucose ($[Glc]_P$) concentrations and ^{13}C fractional enrichment time courses for the two different infusion protocols A and B from one volunteer. For each protocol, the targeted $[Lac]_P$ and fractional enrichment were attained in the first 5 min and their levels remained steady throughout the 2 h infusions. The range of concentration for plasma lactate achieved by the two infusion protocols (A and B) was 0.8 to 2.8 mmol/L, whereas the range of steady-state fractional enrichment of [3-^{13}C]lactate in plasma achieved was 23.0–50.4% with a mean value of 36.2 ± 0.9% (mean ± SD; $n = 9$). It is important to note that circulating [3-^{13}C]lactate is metabolized by the liver and will transfer ^{13}C label into glucose through gluconeogenesis (Cohen, 1987; Rothman et al., 1991; Lebon et al., 2002). As determined by gas chromatography–mass spectroscopy of blood samples, the incorporation of ^{13}C label into the C1, C2, C5, and C6 positions of plasma glucose were found to be significant for the C1 and C6 positions with similar fractional enrichments over natural abundance at the end of the infusion: 3.9 ± 0.7% for C1 and 3.5 ± 0.6% for C6 (mean ± SD; $n = 9$). To take into account the contribution of ^{13}C-labeled glucose to the measured time courses, ^{13}C-glucose time courses have been incorporated to the modeling as an input function.

Brain ^{13}C-labeled metabolite quantification

Figure 3 shows a steady-state spectrum from one of the volunteers, obtained from the last 32 min of a 2 h [3-^{13}C]lactate infusion study as well as its decomposition by LCModel. As described, the multiple positions of glutamate, glutamine, and aspartate are well resolved with typical Cramér–Rao lower bounds values (CRLB) at the end of the study being <5% for GluC4, <15% for GluC3, GlnC4, GluC2, and AspC3, and <25% for NAAC3, GlnC3, and GlnC2. However, to improve the detection and quantification of [3-^{13}C]lactate signal (LacC3) at 21 ppm, we assumed a rapid establishment of a steady brain lactate concentration and used the sum of all spectra acquired over the 2 h of infusion. This way, the LacC3 peak was detected and quantified with CRLB between 9 and 30%.

Comparison of steady-state labeling from [3-^{13}C]lactate with [2-^{13}C]acetate and [1-^{13}C]glucose

To assess whether the oxidation of lactate is primarily glial, or instead is similar to that of glucose, we compared the labeling from a 2 h [3-^{13}C]lactate infusion with labeling from [1-^{13}C]glucose and [2-^{13}C]acetate. The steady-state spectrum presented in Figure 4*a* may be compared with that acquired from the same volunteer after [1-^{13}C]glucose (Fig. 4*b*) and [2-^{13}C]acetate infusions (Fig. 4*c*). The spectra were scaled based on their natural abundance peaks of NAAC3. Although the high labeling of GlnC4 resonance for the acetate infusion reflects clearly the compartmentation of acetate oxidization in glia (Hassel et al., 1995; Bachelard, 1998; Lebon et al., 2002), the pattern of labeling for glucose and lactate infusions are very similar except for the minimal ^{13}C-^{13}C sidebands to the glutamate and glutamine resonances. The ^{13}C-^{13}C sidebands that would result from doubly labeled molecules are not observable because of the low fractional labeling of acetyl-CoA after the lactate infusion (Table 1). To account for these undetected resonances small correction factors (~1.04 for GluC4 and GluC2; ~1.11 for GluC3) were applied. As can be seen in Table 1, the [4-^{13}C]glutamine/[4-^{13}C]glutamate (fe[GlnC4]/fe[GluC4]) labeling ratio extracted from our set of [3-^{13}C]lactate infusions (0.78 ± 0.04; $n = 9$) does not differ significantly ($p = 0.14$, Kolmogorov–Smirnov two-sample test) from the one obtained with [1-^{13}C]glucose infusions (0.87 ± 0.04; $n = 7$). In contrast, there is a large difference in labeling with the results from the [2-^{13}C]acetate infusions ($p = 1$, Kolmogorov–Smirnov two-sample test), which exhibit a much higher fe[GlnC4]/fe[GluC4] ratio (2.90 ± 0.22; $n = 7$).

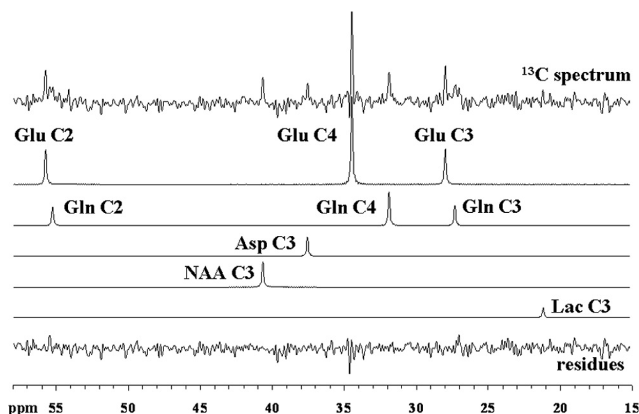

Figure 3. Localized ^{13}C spectrum acquired from the occipito-parietal lobe of a volunteer during the last 32 min of a 2 h [3-^{13}C]lactate infusion study and its decomposition by LCModel. Singlets for GluC4, GluC3, GluC2, GlnC4, GlnC3, GlnC2, AspC3, LacC3, NAAC3, and the residues are displayed. For processing parameters, see Materials and Methods.

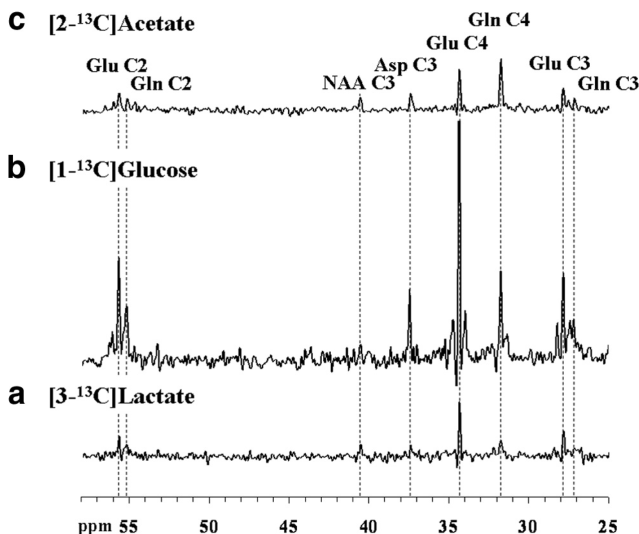

Figure 4. ***a–c***, Localized ^{13}C spectra acquired from the occipito-parietal lobe of the same volunteer either during the last 25 min of a 2 h [3-^{13}C]lactate infusion study ($[Lac]_P \sim 1.5$ mmol/L and ^{13}C FE $\sim$ 29%) (***a***, bottom), during the last 15 min of a 2 h [1-^{13}C]glucose (***b***, middle), or the last 25 min of a 2 h [2-^{13}C]acetate infusion (***c***, top), scaled to exhibit the differences in ^{13}C fractional enrichment reached for glutamate and glutamine. For processing parameters, see Materials and Methods.

Metabolic modeling and TCA flux determinations

Figure 5, *a* and *b*, displays the measured GluC4, GluC3, GluC2, GlnC4, GlnC3, GlnC2 time courses as well as the corresponding best fits obtained for one individual experiment. The resulting fluxes were $V_{TCAn} = 0.50 \pm 0.02$ μmol $\cdot$ g^{-1} $\cdot$ min^{-1} and $V_{TCAg} = 0.15 \pm 0.02$ μmol $\cdot$ g^{-1} $\cdot$ min^{-1} (mean $\pm$ SD; $n = 9$). These values are consistent with values reported previously (Mason et al., 1999; Shen et al., 1999; Chen et al., 2001; Chhina et al., 2001; Blüml et al., 2002; Lebon et al., 2002). The overall TCA cycle rate is 0.65 μmol $\cdot$ g^{-1} $\cdot$ min^{-1}, which is in the low range for the values of total V_{TCA} reported for humans, the range being [0.57; 0.83] (for review, see Hyder et al., 2006). We believe the explanation for the lower rate is the higher contribution of white matter to our volume of interest ($\sim$53% white matter). Indeed, previous MRS studies have established a threefold to fourfold lower TCA cycle rate in white matter compared with gray matter in human (Mason et al., 1999) and rat (de Graaf et al., 2004). We have obtained

Table 1. ^{13}C fractional enrichment of glutamate and glutamine in positions C4 and C3 for [2-^{13}C]acetate, [1-^{13}C]glucose, and [3-^{13}C]lactate infusions in the human occipito-parietal lobe at the end of 2 h of infusions

	[3-^{13}C]Lactate	[1-^{13}C]Glucose	[2-^{13}C]Acetate
fe[GluC4]	6.7 ± 0.6	19.4 ± 1.2	5.4 ± 0.5
fe[GluC3]	4.7 ± 0.4	14.7 ± 0.8	5.0 ± 0.5
fe[GlnC4]	5.2 ± 0.6	16.7 ± 0.8	16.0 ± 2.4
fe[GlnC3]	3.7 ± 0.4	12.0 ± 0.7	7.9 ± 1.0
fe[GlnC4]/fe[GluC4]	0.78 ± 0.04	0.87 ± 0.04*	2.90 ± 0.22**

At the bottom line, the [4-^{13}C]glutamine/[4-^{13}C]glutamate labeling ratio is calculated for each individual experiment and averaged. Fractional enrichment values are in percentage, means $\pm$ SD, $n = 9$ for lactate group and $n = 7$ for the glucose and acetate group. The natural abundance (1.1%) is not subtracted.

Kolmogorov–Smirnov two-sample tests for difference between lactate and other groups: $^*p = 0.14$ with glucose, and $^{**}p = 1$ with acetate.

similar rates of metabolism using ^{13}C-labeled glucose and acetate as tracers from this same volume (Boumezbeur et al., 2010).

Determination of lactate transport kinetics and net rate of lactate consumption

The measured values of V_{in}, $[Lac]_B$, and CMRlac are displayed in Figure 6*a–c* along with their respective linear regressions. The following linear relationships were obtained: $V_{in} = 0.042.[Lac]_P$ ($R^2 = 0.58$); $[Lac]_B = 0.63.[Lac]_P$ ($R^2 = 0.75$), and CMRlac $= 0.019.[Lac]_P$-0.007 ($R^2 = 0.71$). To determine the range of values of V_{MAX} and K_T consistent with the results, the curves were fit to the reversible Michaelis–Menten model as described above and Monte Carlo analysis performed to determine the range of values consistent with the data. Based on this analysis, the mean value of K_T was 5.1 mmol/L with a 68% confidence interval (CI) ranging from 2.4 to 7.8 mmol/L. As shown in Figure 6*d*, the distribution of K_T is not symmetrical with a skewness (G_1) of 0.5. The mean and range of K_T values are consistent with V_{in} being close to linear with the range of plasma lactate concentration studied (0.8–2.8 mmol/L), which encompasses the full range encountered in most physiological conditions. The mean value of V_{MAX} was calculated to be $V_{MAX} = 0.40 \pm 0.13$ μmol $\cdot$ g^{-1} $\cdot$ min^{-1}. The overlay of the probability density functions and corresponding histograms for K_T and V_{MAX} are shown in Figure 6*d*.

Because the initial run of the metabolic modeling was performed assuming a K_T value of 4.4 mmol/L, the metabolic modeling was performed again with K_T set the following values: 2.4, 5.1, and 7.8 mmol/L corresponding to a 68% centered confidence interval. Consistent with the relationships of Equations 7 and 10, the V_{in} and CMRlac values were found to remain mostly unchanged, as demonstrated by Figure 7, *a* and *b*, in which individuals fluxes values obtained for $K_T = 2.4$ and 7.8 mmol/L are compared (slopes $\sim$ 1.01; $R^2 > 0.99$). Table 2 presents the V_{MAX} and V_{MAX}/K_T ratios derived from the metabolic modeling of the individual datasets (mean $\pm$ SD; $n = 9$) for the different K_T values considered.

Discussion

Over the past decade, ^{13}C MRS has been used to study cerebral metabolism *in vivo* mostly using ^{13}C-labeled glucose (for review, see Shen and Rothman, 2002; Hyder et al., 2006). However several studies have looked at the alternate substrates: acetate and β-hydroxybutyrate (Pan et al., 2001; Lebon et al., 2002). The results here demonstrate that ^{13}C-labeled lactate can be used to study brain metabolism, and also establish lactate transport parameters and cell type preference for its consumption. In addition, they support that plasma lactate can potentially be a significant net fuel for brain metabolism under conditions of elevated plasma lactate or decreased plasma glucose.

Contribution of plasma lactate to brain metabolism

Using the measured values of plasma and intracellular lactate and V_{in}, CMRlac was estimated using Equation 7 and is plotted in Figure 6*c*. At plasma lactate levels close to resting values, there is very little if any net consumption, consistent with previous arteriovenous (AV) difference studies (Siesjö, 1978). As plasma lactate concentration is elevated, CMRlac increases linearly with a ratio of CMRlac/V_{TCA} ~ 7% for the highest plasma lactate concentration studied ($[Lac]_P$ = 2.8 mmol/L). Although CMRlac is relatively low, our results suggest that an additional increase in $[Lac]_P$ or a decrease in $[Lac]_B$ can lead to substantially higher contributions to metabolism. Smith et al. (2003) found plasma lactate was able to replace ~17% of glucose uptake after blood lactate was elevated by lactate infusion corresponding to CMRlac ~ 0.08 $\mu mol \cdot g^{-1} \cdot min^{-1}$ for $[Lac]_P$ ~ 4.1 mmol/L at euglycemia. Using either the best linear fit to CMRlac or the mean K_T and V_{MAX} to extrapolate to this higher lactate concentration, a CMRlac flux of 0.07 $\mu mol \cdot g^{-1} \cdot min^{-1}$ is predicted, consistent with the measurement by Smith et al. (2003). Studies have also shown high net lactate usage when it is elevated by hypoxia (Schurr et al., 1997a,b) or after intense physical exercise (Kemppainen et al., 2005; van Hall et al., 2009).

The maximum rate of CMRlac as a function of $[Lac]_P$ can be determined from Equations 7 and 8 with the assumption that intracellular lactate concentration is maintained near 0 by metabolism. In this case, CMRlac is equivalent to V_{in} as follows:

$$\max \mathrm{CMRlac} = V_{in}\big|_{[Lac]_B=0} = \frac{V_{MAX}}{K_T/[Lac]_P + 1}. \quad (11)$$

The maximum rate is relevant for situations in which $[Lac]_B$ is low because of reduced glycolytic lactate production, which may occur during hypoglycemia. Figure 8 plots the maximum CMRlac versus $[Lac]_P$ for the mean K_T value and the values at the 68% CI. Above the mean value, there is very little influence of K_T on the calculated maximum CMRlac. The mean value of V_{MAX} was used. Under these conditions, the maximum contribution of plasma lactate to brain metabolism under normal plasma lactate concentrations near 1.0 mmol/L is predicted to be CMRlac/V_{TCA} ~ 10%. This contribution to brain energy production would be highly significant for avoiding brain energy failure under conditions of hypoglycemia that occur during fasting and for patients with type 1 diabetes after insulin injection, particularly if brain lactate transport is upregulated by twofold as it has been reported for acetate by Mason et al. (2006). The V_{MAX} for plasma lactate transport is high and in principle could provide for as much as ~60% of the oxidative substrate needs of the occipital cortex at very high plasma levels (CMRlac = V_{MAX}). Brain metabolism of plasma lactate could conceivably differ in other brain regions reflecting differences in activity of the relevant monocarboxylic acid transporters.

In the study by van Hall et al. (2009), circulating lactate brain uptake and subsequent contribution to oxidative energy synthesis was estimated using AV difference. The brain went from a net release of lactate at rest ($[Lac]_P$ = 0.9 mmol/L), to a net consumer during lactate infusion at levels of $[Lac]_P$ = 3.9 mmol/L and $[Lac]_P$ = 6.9 mmol/L. These results are consistent with our predictions of net lactate consumption as a function of $[Lac]_P$. The lactate they infused was ^{13}C-enriched at the C1 position and they

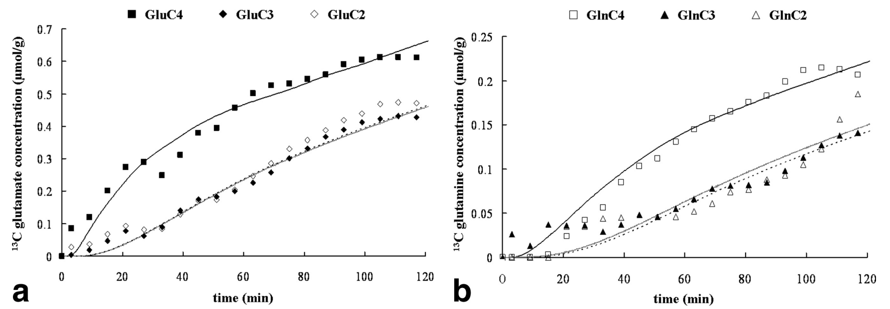

Figure 5. ***a***, ***b***, Time courses of glutamate (***a***) and glutamine (***b***) ^{13}C concentrations for the C4, C3, and C2 positions from one of the subjects during the infusion of [3-^{13}C]lactate ($[Lac]_P$ ~ 2.7 mmol/L and ^{13}C FE ~ 50%). The glutamate and glutamine C4 labeling are represented by squares (closed and open, respectively), whereas the glutamate C3 and C2 labeling, by diamonds (closed and open, respectively), and glutamine C3 and C2 labeling, by triangles (closed and open, respectively). The lines are the fits obtained with the metabolic model (solid, C4; dashed, C3; shaded, C2 positions). The scale for glutamine is increased approximately by a factor of 3 to facilitate the visualization of the kinetics.

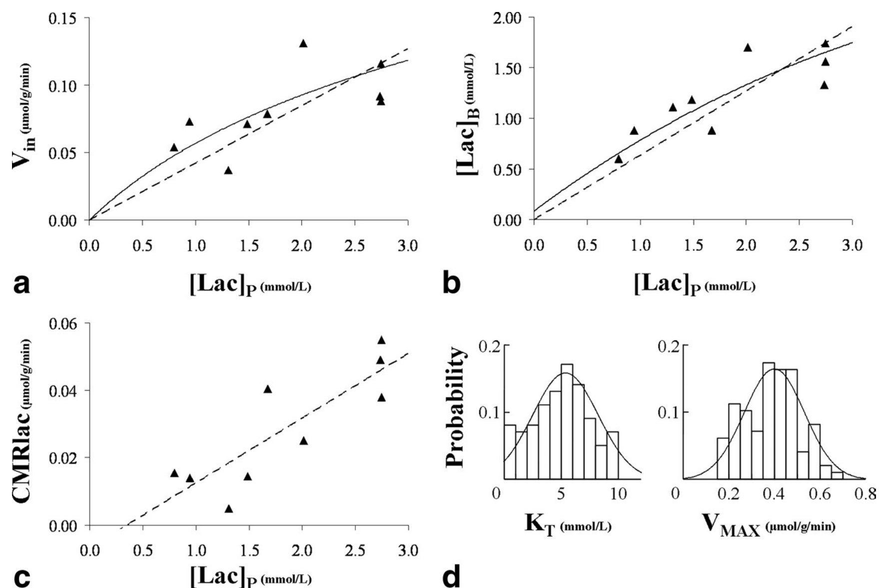

Figure 6. ***a***, Lactate influx plotted as a function of the plasma lactate concentration. The dashed straight line represents the linear regression that has a slope of 0.042 and a R^2 value of 0.58. ***b***, Brain lactate as a function of the plasma lactate concentration. The dashed straight line represents the linear regression that has a slope of 0.63 and a R^2 value of 0.75. For both ***a*** and ***b***, the solid curve line represents the best fit obtained from a least-square minimization using expressions in Equations 5 and 8 given by the reversible Michaelis–Menten model. ***c***, Lactate net consumption plotted as a function of the plasma lactate concentration. The dashed straight line represents the linear regression: CMRlac (in micromoles per gram per minute) = 0.019.$[Lac]_P$-0.007, R^2 = 0.72. ***d***, Overlay of the probability density functions and corresponding histograms for K_T and V_{MAX} values derived from the Monte Carlo analysis (for details, see Materials and Methods) of the data presented in ***a*** and ***b***: K_T = 5.1 ± 2.7 mmol/L and V_{MAX} = 0.40 ± 0.13 $\mu mol \cdot g^{-1} \cdot min^{-1}$ (mean ± SD).

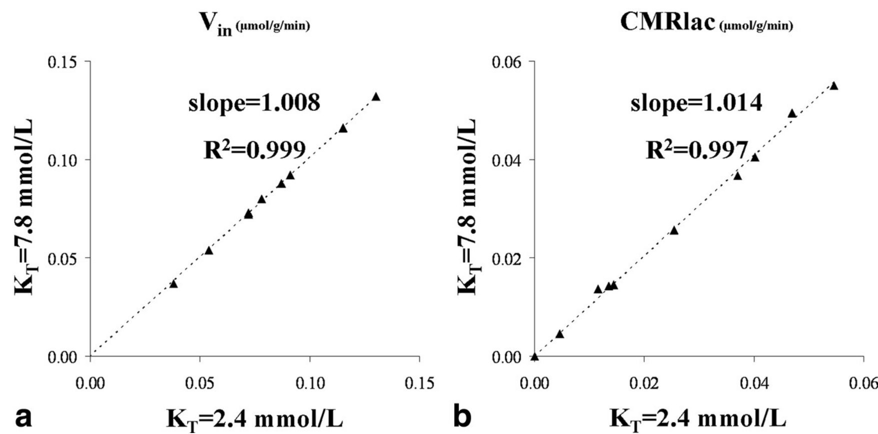

Figure 7. ***a***, ***b***, Lactate influx values (***a***) and net consumption of lactate (***b***) obtained from the dynamic modeling of the data assuming K_T being either equal to the mean − SD = 2.4 or mean + SD = 7.8 mmol/L (as determined from the Monte Carlo simulations). The impact observed on the estimated V_{in} and CMRlac values is negligible as illustrated by the slopes (~1.01) and R^2 coefficients (>0.99) of the linear regressions.

Table 2. V_{MAX} values and V_{MAX}/K_T ratio obtained from the dynamic modeling of the individual datasets (mean ± SD; $n = 9$) for K_T values being 2.4, 5.1, and 7.8 mmol/L

	K_T (mmol/L)		
	Mean − SD 2.4	Mean 5.1	Mean + SD 7.8
V_{MAX} (μmol · g^{-1} · min^{-1})	0.25 ± 0.07	0.38 ± 0.10	0.50 ± 0.15
V_{MAX}/K_T (/min)	0.104 ± 0.028	0.074 ± 0.021	0.065 ± 0.019

These K_T values correspond to the mean − SD, mean, and mean + SD values estimated from the Monte Carlo analysis (Fig. 6*d*).

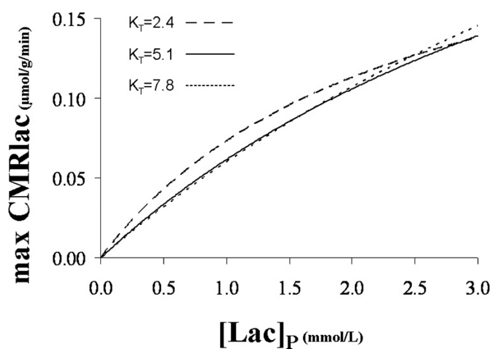

Figure 8. Maximum lactate consumption versus plasma lactate concentration for the mean K_T value, 5.1 mmol/L, and the values at the 68% CI, 2.4 and 7.8 mmol/L. For each K_T value, the corresponding mean V_{MAX} value was considered: 0.25, 0.38, and 0.50 μmol · g^{-1} · min^{-1} (Table 2).

assessed the fraction of lactate oxidized and its contribution to cerebral energy expenditure based on the appearance of the ^{13}C label in CO_2. At the three concentrations studied, they measured a contribution of lactate to total cerebral oxidative energy expenditure of 8, 19, and 27%, which is in excellent agreement with the ratio calculated between the lactate entry and brain TCA cycle rates (V_{in}/V_{TCA}) using our measured kinetic parameters (K_T = 5.1 mmol/L; V_{MAX} = 0.38 μmol · g^{-1} · min^{-1}): 8, 21, and 28%. This agreement is attributable to the relative ^{13}C labeling of CO_2 through PDH (pyruvate dehydrogenase) activity being proportional to the fractional enrichment of brain lactate/pyruvate pool (Eq. 9). We also note that the good agreement with AV difference studies suggests that our values obtained from the occipital lobe may be extrapolated to the cerebral cortex as a whole, although direct measurements will be needed to establish the generality conclusively.

Cellular compartmentation of lactate metabolism

Because glutamine is synthesized only in glial cells, whereas the majority of glutamate resides in neurons, analysis of [4-^{13}C]glutamine/[4-^{13}C]glutamate (fe[GlnC4]/fe[GluC4]) labeling ratios can give an insight into the metabolic compartmentation of a substrate (Pan et al., 2002), with higher ratios indicating greater percentages of substrate transport and oxidation in glia. In our study, this ratio for lactate as a substrate was 0.78 ± 0.04 (mean ± SD; $n = 9$), similar to the ratio determined for [1-^{13}C]glucose as substrate: 0.87 ± 0.04 (mean ± SD; $n = 7$). In both cases, the ratios were determined for the same occipito-parietal location and from a matched group of healthy young subjects, consistent with the same distribution of usage in glia and neurons.

In contrast, studies using [2-^{13}C]acetate, a known glial substrate, exhibit fe[GlnC4]/fe[GluC4] ratios severalfold higher. Based on previous ^{13}C MRS studies that quantitated neuronal and glial glucose oxidation, the finding of similar labeling as observed with [1-^{13}C] glucose suggests that there is similarly a fourfold higher oxidation of plasma lactate in neurons than glia (Lebon et al., 2002; Boumezbeur et al., 2010). However, a study using high-resolution [^{14}C]2-deoxyglucose autoradiography in combination with immune staining of neuronal and glial cell bodies suggested that glucose uptake is evenly distributed between these cell types (Nehlig et al., 2004). The [^{14}C]2-deoxyglucose findings, which reflects total glucose uptake rather than oxidation, would not conflict with the present MRS findings should the lactate produced through glial glycolysis be oxidized mainly in the neurons, a point made by the study's authors (Nehlig et al., 2004).

Recent studies suggest that lactate is more specific to neurons than glucose (Qu et al., 2000; Tyson et al., 2003). For example, Tyson et al. (2003) measured fe[GlnC4]/fe[GluC4] ratios closer to 0.67 for lactate versus 0.92 for glucose. A potential explanation for this discrepancy is that, as discussed previously, glucose labeled at the C1 and C6 positions produced by gluconeogenesis from [3-^{13}C]lactate resulted in labeling of brain glutamine and glutamate, obscuring the difference. Alternatively, it may reflect species differences. For now, we can only definitively conclude that, at minimum, plasma lactate is used by neurons and glia at a fraction similar to that of plasma glucose.

Evaluation of lactate transport kinetics

Kinetics for lactate transport were evaluated using a reversible Michaelis–Menten model. The reversible Michaelis–Menten kinetics have been described in detail previously (Mahler and Cordes, 1971; Cunningham et al., 1986) and used successfully to study glucose transport kinetics in human brain (Gruetter et al., 1998; Choi et al., 2001; de Graaf et al., 2001). Detailed kinetic modeling and meta-analysis of literature results by Simpson et al. (2007) have supported it as accurately describing brain glucose and monocarboxylic acid transport. As seen in Figure 6*a*, V_{in} is close to linear with $[Lac]_P$ over the range studied. The mean K_T of 5.1 mmol/L determined by Monte Carlo analysis agrees with this

observation, although there is a significant spread in the range of values consistent with results from previous studies of MCT_1 in animal brain or oocytes, which have found K_T values of ~4 mmol/L (Bröer et al., 1998; Manning Fox et al., 2000).

Relevance to the astrocyte-to-neuron lactate shuttle

A major question regarding lactate metabolism is whether lactate produced in astrocytes by glycolysis is transferred to neurons for oxidation, often called the astrocyte-to-neuron lactate shuttle (ANLS). Although there is considerable evidence for the ANLS model (Magistretti et al., 1999; Pellerin et al., 2005), it remains to be shown directly that there is net transfer of lactate from glia to neurons *in vivo*. A prediction of the ANLS model is that lactate transport capacities of neurons and astrocytes are high enough to meet the energy demand of neurons. The finding that relative labeling of glutamine and glutamate from plasma-borne [3-^{13}C]lactate is similar to that from [1-^{13}C]glucose as substrate strongly suggests that neuronal and glial lactate pools have the same ^{13}C fractional enrichment, implying that the relative lactate transport capacity of neurons and astroglia is either the same as their relative rates of glucose oxidation or much greater, creating effectively a single-shared lactate pool. Combined with the finding extrapolated from transport kinetics that plasma lactate can provide up to 60% of the brain's oxidative requirements, our results suggest that cellular lactate transport is not likely to be limiting for an ANLS mechanism in human cerebral cortex.

Evaluation of ^{13}C-labeled lactate as a metabolic tracer

As a general MRS tracer for studying brain metabolism, the primary limitation of lactate is that its labeling of the brain pyruvate pool is relatively low at physiological levels. For example, as shown in Figure 4, severalfold higher ^{13}C fractional enrichment was achieved using [1-^{13}C]glucose rather than even the higher level of lactate in the present study. A second limitation of using lactate is that the production of labeled glucose from [3-^{13}C]lactate via gluconeogenesis by liver is a potential complication in the metabolic modeling. Significant labeling of glucose in the C1 or C6 position was observed (2.8 ± 0.7% for C1 and 2.4 ± 0.6% for C6 above natural abundance; mean ± SD; $n = 9$). Because of the delay in the appearance of glucose labeling (Fig. 2*d*) and our incorporation of labeled glucose as a precursor in the metabolic modeling, its impact on the determination of metabolic rates and transport kinetics was not large. However, it may have obscured subtle differences between the cellular localization of lactate and glucose utilization. A potential solution would be the administration of insulin during the experiment to slow down the release in the bloodstream of labeled glucose from the liver. A final limitation is that elevated plasma sodium lactate is a well known anxiogen used experimentally to provoke and study panic disorder (Cowley and Arana, 1990). In the present set of experiments, subjects did not report any symptoms related to anxiety during the infusion, most likely because of the low plasma lactate concentrations used. However, care must be taken for this possibility, which may restrict the level of lactate that can be explored experimentally.

Conclusion

In conclusion, the V_{MAX} and K_T of lactate metabolism demonstrate that the human brain has the capacity to support up to 10% of its energy metabolism with lactate under physiological levels and up to 60% under supraphysiological levels. The unidirectional transport of lactate is effectively linear over the physiological range and beyond. Neurons are the dominant source of plasma lactate metabolism, similar to what is observed with plasma glucose. Plasma lactate may be a significant net fuel for brain metabolism under conditions in which plasma lactate is elevated such as after exercise or hypoxia/ischemia or when plasma glucose is reduced because of fasting hypoglycemia or after insulin administration. ^{13}C MRS has the potential of directly studying brain lactate metabolism in these and other states in which plasma lactate may play an important role in sustaining brain function.

References

Bachelard H (1998) Landmarks in the application of ^{13}C-magnetic resonance spectroscopy to studies of neuronal/glial relationships. Dev Neurosci 20:277–288.

Blüml S, Moreno-Torres A, Shic F, Nguy CH, Ross BD (2002) Tricarboxylic acid cycle of glia in the in vivo human brain. NMR Biomed 15:1–5.

Boumezbeur F, Mason GF, de Graaf RA, Behar KL, Cline GW, Shulman GI, Rothman DL, Petersen KF (2010) Altered brain mitochondrial metabolism in healthy aging as assessed by *in vivo* magnetic resonance spectroscopy. J Cereb Blood Flow Metab 30:211–221.

Bröer S, Schneider HP, Bröer A, Rahman B, Hamprecht B, Deitmer JW (1998) Characterization of the monocarboxylate transporter 1 expressed in *Xenopus laevis* oocytes by changes in cytosolic pH. Biochem J 333:167–174.

Chen W, Zhu XH, Gruetter R, Seaquist ER, Adriany G, Uğurbil K (2001) Study of tricarboxylic acid cycle flux changes in human visual cortex during hemifield visual stimulation using ^{1}H-[^{13}C] MRS and fMRI. Magn Reson Med 45:349–355.

Chhina N, Kuestermann E, Halliday J, Simpson LJ, Macdonald IA, Bachelard HS, Morris PG (2001) Measurement of human tricarboxylic acid cycle rates during visual activation by ^{13}C magnetic resonance spectroscopy. J Neurosci Res 66:737–746.

Choi IY, Lee SP, Kim SG, Gruetter R (2001) In vivo measurements of brain glucose transport using the reversible Michaelis–Menten model and simultaneous measurements of cerebral blood flow changes during hypoglycemia. J Cereb Blood Flow Metab 21:653–663.

Cohen SM (1987) ^{13}C NMR study of effects of fasting and diabetes on the metabolism of pyruvate in the tricarboxylic acid cycle and the utilization of pyruvate and ethanol in lipogenesis in perfused rat liver. Biochemistry 26:573–580.

Cowley DS, Arana GW (1990) The diagnostic utility of lactate sensitivity in panic disorder. Arch Gen Psychiatry 47:277–284.

Cunningham VJ, Hargreaves RJ, Pelling D, Moorhouse SR (1986) Regional blood-brain glucose transfer in the rat: a novel double-membrane kinetic analysis. J Cereb Blood Flow Metab 6:305–314.

de Graaf RA, Pan JW, Telang F, Lee JH, Brown P, Novotny EJ, Hetherington HP, Rothman DL (2001) Differentiation of glucose transport in human brain gray and white matter. J Cereb Blood Flow Metab 21:483–492.

de Graaf RA, Mason GF, Patel AB, Rothman DL, Behar KL (2004) Regional glucose metabolism and neurotransmission in rat brain *in vivo*. Proc Natl Acad Sci U S A 101:12700–12705.

Gjedde A, Diemer NH (1983) Autoradiographic determination of regional brain glucose content. J Cereb Blood Flow Metab 3:303–310.

Gruetter R, Novotny EJ, Boulware SD, Mason GF, Rothman DL, Shulman GI, Prichard JW, Shulman RG (1994) Localized ^{13}C NMR spectroscopy in the human brain of amino acid labeling from D-[1-^{13}C]glucose. J Neurochem 63:1377–1385.

Gruetter R, Novotny EJ, Boulware SD, Rothman DL, Shulman RG (1996) ^{1}H NMR studies of glucose transport in the human brain. J Cereb Blood Flow Metab 16:427–438.

Gruetter R, Uğurbil K, Seaquist ER (1998) Steady-state cerebral glucose concentrations and transport in the human brain. J Neurochem 70:397–408.

Gruetter R, Seaquist ER, Uğurbil K (2001) A mathematical model of compartmentalized neurotransmitter metabolism in the human brain. Am J Physiol Endocrinol Metab 281:E100–E112.

Harada M, Okuda C, Sawa T, Murakami T (1992) Cerebral extracellular glucose and lactate concentration during and after moderate hypoxia in glucose- and saline-infused rats. Anesthesiology 77:728–734.

Hassel B, Sonnewald U, Fonnum F (1995) Glial-neuronal interactions as

studied by cerebral metabolism of [2-^{13}C]acetate and [1-^{13}C]glucose: an *ex vivo* ^{13}C NMR spectroscopic study. J Neurochem 64:2773–2782.

Henry PG, Oz G, Provencher S, Gruetter R (2003) Toward dynamic isotopomer analysis in the rat brain *in vivo*: automatic quantitation of ^{13}C NMR spectra using LCModel. NMR Biomed 16:400–412.

Henry PG, Adriany G, Deelchand D, Gruetter R, Marjanska M, Öz G, Seaquist ER, Shestov A, Uğurbil K (2006) In vivo ^{13}C NMR spectroscopy and metabolic modeling in the brain: a practical perspective. Magn Reson Imaging 24:527–539.

Hetherington HP, Pan JW, Mason GF, Adams D, Vaughn MJ, Twieg DB, Pohost GM (1996) Quantitative high-resolution spectroscopic imaging of human brain *in vivo* at 4.1T using image segmentation. Magn Reson Med 36:21–29.

Hyder F, Patel AB, Gjedde A, Rothman DL, Behar KL, Shulman RG (2006) Neuronal-glial glucose oxidation and glutamatergic-GABAergic function. J Cereb Blood Flow Metab 26:865–877.

Kemppainen J, Aalto S, Fujimoto T, Kalliokoski KK, Långsjö J, Oikonen V, Rinne J, Nuutila P, Knuuti J 2005 High intensity exercise decreases global brain glucose uptake in humans. J Physiol 568:323–332.

Lebon V, Petersen KF, Cline GW, Shen J, Mason GF, Dufour S, Behar KL, Shulman GI, Rothman DL (2002) Astroglial contribution to brain energy metabolism in humans revealed by ^{13}C nuclear magnetic resonance spectroscopy: elucidation of the dominant pathway for neurotransmitter glutamate repletion and measurement of astrocytic oxidative metabolism. J Neurosci 22:1523–1531.

Leenders KL, Perani D, Lammertsma AA, Heather JD, Buckingham P, Healy MJ, Gibbs JM, Wise RJ, Hatazawa J, Herold S, Beaney RP, Brooks DJ, Spinks T, Rhodes C, Frackowiak RSJ, Jones T (1990) Cerebral blood flow, blood volume and oxygen utilization. Normal values and effect of age. Brain 113:27–47.

Lin AP, Shic F, Enriquez C, Ross BD (2003) Reduced glutamate neurotransmission in patients with Alzheimer's disease—an *in vivo* ^{13}C magnetic resonance spectroscopy study. MAGMA 16:29–42.

Magistretti PJ, Pellerin L, Rothman DL, Shulman RG (1999) Energy on demand. Science 283:496–497.

Mahler H, Cordes E (1971) Biological chemistry. New York: Harper and Row.

Mangia S, Tkáč I, Gruetter R, Van De Moortele PF, Giove F, Maraviglia B, Uğurbil K (2006) Sensitivity of single-voxel ^{1}H-MRS in investigating the metabolism of the activated human visual cortex at 7 T. Magn Reson Imaging 24:343–348.

Manning Fox JE, Meredith D, Halestrap AP (2000) Characterisation of human monocarboxylate transporter 4 substantiates its role in lactic acid efflux from skeletal muscle. J Physiol 529:285–293.

Maran A, Cranston I, Lomas J, Macdonald I, Amiel SA (1994) Protection by lactate of cerebral function during hypoglycaemia. Lancet 343:16–20.

Mason GF, Rothman DL (2002) Graded image segmentation of brain tissue in the presence of inhomogeneous radio frequency fields. Magn Reson Imaging 20:431–436.

Mason GF, Rothman DL, Behar KL, Shulman RG (1992) NMR determination of the TCA cycle rate and α-ketoglutarate/glutamate exchange rate in rat brain. J Cereb Blood Flow Metab 12:434–447.

Mason GF, Gruetter R, Rothman DL, Behar KL, Shulman RG, Novotny EJ (1995) Simultaneous determination of the rates of the TCA cycle, glucose utilization, α-ketoglutarate/glutamate exchange, and glutamine synthesis in human brain by NMR. J Cereb Blood Flow Metab 15:12–25.

Mason GF, Pan JW, Chu WJ, Newcomer BR, Zhang Y, Orr R, Hetherington HP (1999) Measurement of the tricarboxylic acid cycle rate in human grey and white matter *in vivo* by ^{1}H-[^{13}C] magnetic resonance spectroscopy at 4.1T. J Cereb Blood Flow Metab 19:1179–1188.

Mason GF, Falk Petersen K, de Graaf RA, Kanamatsu T, Otsuki T, Shulman GI, Rothman DL (2003) A comparison of ^{13}C NMR measurements of the rates of glutamine synthesis and the tricarboxylic acid cycle during oral and intravenous administration of [1-^{13}C]glucose. Brain Res Brain Res Protoc 10:181–190.

Mason GF, Petersen KF, Lebon V, Rothman DL, Shulman GI (2006) Increased brain monocarboxylic acid transport and utilization in type 1 diabetes. Diabetes 55:929–934.

Mason GF, Petersen KF, de Graaf RA, Shulman GI, Rothman DL (2007) Measurements of the anaplerotic rate in the human cerebral cortex using ^{13}C magnetic resonance spectroscopy and [1-^{13}C] and [2-^{13}C]glucose. J Neurochem 100:73–86.

Michaelis T, Merboldt KD, Bruhn H, Hänicke W, Frahm J (1993) Absolute concentrations of metabolites in the adult human brain *in vivo*: quantification of localized proton MR spectra. Radiology 187:219–227.

Nehlig A, Wittendorp-Rechenmann E, Lam CD (2004) Selective uptake of [^{14}C]2-deoxyglucose by neurons and astrocytes: high-resolution microautoradiographic imaging by cellular ^{14}C-trajectography combined with immunohistochemistry. J Cereb Blood Flow Metab 24:1004–1014.

Oldendorf WH (1973) Carrier-mediated bloodbrain barrier transport of short-chain monocarboxylic organic acids. Am J Physiol 224:1450–1453.

Pan JW, Rothman TL, Behar KL, Stein DT, Hetherington HP (2000) Human brain β-hydroxybutyrate and lactate increase in fasting-induced ketosis. J Cereb Blood Flow Metab 20:1502–1507.

Pan JW, Telang FW, Lee JH, de Graaf RA, Rothman DL, Stein DT, Hetherington HP (2001) Measurement of β-hydroxybutyrate in acute hyperketonemia in human brain. J Neurochem 79:539–544.

Pan JW, de Graaf RA, Petersen KF, Shulman GI, Hetherington HP, Rothman DL (2002) [2,4-^{13}C2]-beta-Hydroxybutyrate metabolism in human brain. J Cereb Blood Flow Metab 22:890–898.

Pellerin L, Bergersen LH, Halestrap AP, Pierre K (2005) Cellular and subcellular distribution of monocarboxylate transporters in cultured brain cells and in the adult brain. J Neurosci Res 79:55–64.

Provencher SW (1993) Estimation of metabolite concentrations from localized in vivo proton NMR spectra. Magn Reson Med 30:672–679.

Qu H, Håberg A, Haraldseth O, Unsgård G, Sonnewald U (2000) ^{13}C MR spectroscopy study of lactate as substrate for rat brain. Dev Neurosci 22:429–436.

Rothman DL, Magnusson I, Katz LD, Shulman RG, Shulman GI (1991) Quantitation of hepatic glycogenolysis and gluconeogenesis in fasting humans with ^{13}C NMR. Science 254:573–576.

Rothman DL, Novotny EJ, Shulman GI, Howseman AM, Petroff OA, Mason G, Nixon T, Hanstock CC, Prichard JW, Shulman RG (1992) ^{1}H-[^{13}C] NMR measurements of [4-^{13}C]glutamate turnover in human brain. Proc Natl Acad Sci U S A 89:9603–9606.

Schurr A, Payne RS, Miller JJ, Rigor BM (1997a) Brain lactate, not glucose, fuels the recovery of synaptic function from hypoxia upon reoxygenation: an in vitro study. Brain Res 744:105–111.

Schurr A, Payne RS, Miller JJ, Rigor BM (1997b) Brain lactate is an obligatory aerobic energy substrate for functional recovery after hypoxia: further in vitro validation. J Neurochem 69:423–426.

Shen J, Rothman DL (2002) Magnetic resonance spectroscopic approaches to studying neuronal: glial interactions. Biol Psychiatry 52:694–700.

Shen J, Rycyna RE, Rothman DL (1997) Improvements on an *in vivo* automatic shimming method (FASTERMAP). Magn Reson Med 38:834–839.

Shen J, Petersen KF, Behar KL, Brown P, Nixon TW, Mason GF, Petroff OA, Shulman GI, Shulman RG, Rothman DL (1999) Determination of the rate of the glutamate/glutamine cycle in the human brain by in vivo ^{13}C NMR. Proc Natl Acad Sci U S A 96:8235–8240.

Siesjö BK (1978) Brain energy metabolism. New York: Wiley.

Simpson IA, Carruthers A, Vannucci SJ (2007) Supply and demand in cerebral energy metabolism: the role of nutrient transporters. J Cereb Blood Flow Metab 27:1766–1791.

Smith D, Pernet A, Hallett WA, Bingham E, Marsden PK, Amiel SA (2003) Lactate: a preferred fuel for human brain metabolism in vivo. J Cereb Blood Flow Metab 23:658–664.

Sokoloff L (1989) Circulation and energy metabolism of the brain. In: Basic biochemistry (Siegel GL, Agranoff BW, Albers RW, Molinoff PB, eds), pp 577–578. New York: Raven.

Tyson RL, Gallagher C, Sutherland GR (2003) ^{13}C-labeled substrates and the cerebral metabolic compartmentalization of acetate and lactate. Brain Res 992:43–52.

van Hall G, Strømstad M, Rasmussen P, Jans O, Zaar M, Gam C, Quistorff B, Secher NH, Nielsen HB (2009) Blood lactate is an important energy source for the human brain. J Cereb Blood Flow Metab 29:1121–1129.